Influence of mechanical strain on the electrical properties of flexible organic thin-film transistors

2011 Semicond. Sci. Technol. 26 034005

(http://iopscience.iop.org/0268-1242/26/3/034005)

Semicond. Sci. Technol. **26** (2011) 034005 (5pp) doi:10.1088/0268-1242/26/3/034005

Influence of mechanical strain on the electrical properties of flexible organic thin-film transistors

Fang-Chung Chen[1], **Tzung-Da Chen, Bing-Ruei Zeng and Ya-Wei Chung**

Department of Photonics and Display Institute, National Chiao Tung University, Hsinchu 30010, Taiwan

E-mail: fcchen@mail.nctu.edu.tw

Received 30 September 2010, in final form 16 November 2010
Published 14 February 2011
Online at stacks.iop.org/SST/26/034005

Abstract

In this study, we systematically investigated the bending effect on the electrical properties of flexible organic thin-film transistors (OTFTs) fabricated on stainless steel substrates. We found that the compressive strain resulted in an increased mobility, while the tensile strain degraded the electrical performance. We further used a transfer line method to extract the channel and parasitic resistances under either compressive or tensile strain. The results indicated that the parasitic resistance increased apparently under the tensile bending condition, which probably could be attributed to the damage of the source/drain contacts. Additionally, we deduced that mechanical strains influence the energy barrier height between the grains of pentacene thin films, thereby resulting in the variation of channel resistances. Overall, the flexible OTFTs fabricated on the metal foils exhibited high mechanical flexibility and stability.

(Some figures in this article are in colour only in the electronic version)

1. Introduction

Organic thin-film transistors (OTFTs) have received much attention because of their potential applications on low-cost, light-weight, and large-area electronic devices, such as smart cards, paper-like displays, and radio-frequency identification tags [1–5]. In particular, the mechanical flexibility of organic materials facilitates the preparation of organic devices using a high-throughput technique, such as roll-to-roll processing on flexible substrates. At present, flexible OTFTs have been widely reported [6–12]. Among these flexible devices, most of them were fabricated on plastic substrates, such as polyethylene terephthalate and polyethylenenaphthalate films [6–8]. On the other hand, metal foils, such as stainless steel (SS) substrates, are also gaining great interest in the field of flexible electronics due to their excellent mechanical properties, thermal stability and chemical robustness. The low oxygen and moisture permeability can provide effective protection from possible oxidation reactions [9–12]. OTFTs made on SS substrates, however, have been seldom reported. Further, a thorough analysis of the electrical properties of these OTFTs under bending conditions still remains rare. In this work, with the use of pentacene as the semiconducting material, and poly(vinyl cinnamate) (PVCN) [13] as the insulator, we fabricated flexible OTFTs on SS substrates. The bending properties of these devices were systematically investigated. We found that compressive strain resulted in an increased mobility, while tensile strain degraded the electrical performance. From the extracted resistance, we deduced that the compressive strain forced the pentacene grains to become more compact, thereby facilitating the charge transport in the grain boundaries. On the other hand, the tensile strain caused an increase in the spacing between the grains, thereby increasing the energy barrier height for charge hopping. Overall, the flexible OTFTs fabricated on the metal foils exhibited high mechanical flexibility and stability.

2. Experimental details

The device structure is illustrated in figure 1. To fabricate flexible OTFTs on SS substrates, a thick photoresist (EOC-130B) layer was first spin-coated to planarize the surface of the SS foils [12]. Subsequently, a layer of polyimide was also fabricated onto the photoresist layer to modify

[1] Author to whom any correspondence should be addressed.

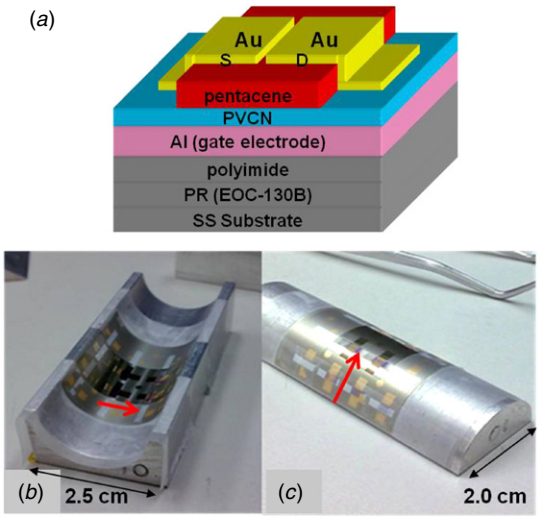

Figure 1. (*a*) The device structure and materials used in this study. The schematic presentation of the bending test apparatus: (*b*) compressive and (*c*) tensile bending. The arrow indicates the direction of the charge transport.

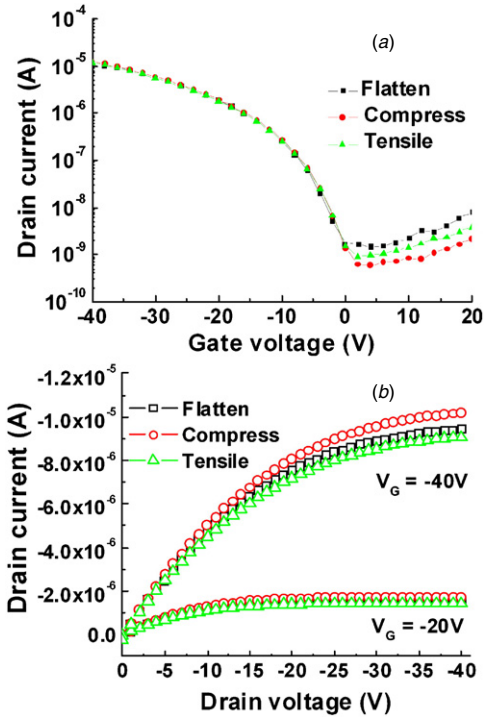

Figure 2. (*a*) The transfer characteristics of the devices measured under different bending conditions. (*b*) The output characteristics of the devices measured under different bending conditions.

the surface energy for improving the adhesion of the upper layers on the substrate. Then, Al was thermally evaporated through a shadow mask to function as the gate electrode. For the dielectric layer, PVCN was firstly dissolved in dichlorobenzene (15 wt%) and was spin coated on the substrates. After a drying process at 80 °C for 10 min, the sample was irradiated with UV light ($\lambda = 264$ nm) to crosslink the PVCN layer [13]. The substrate was then etched by propylene glycol monomethyl ether acetate to define the insulating area. After the etching process, the substrate was dried at 80 °C for 10 min. The thickness of the resulting PVCN layer was ∼400 nm. The measured capacitance was 6.12×10^{-9} F cm^{-2} [14]. For the semiconducting layer, pentacene was thermally deposited (80 nm) on top of the PVCN layer. Finally, Au electrodes were evaporated to serve as the source/drain electrodes. We used a shadow mask to define channel length (L) and width (W). The W/L ratio was kept at 20. The electrical characteristics were measure by Keithley 4200 in ambient air and at room temperature. For the bending tests, the devices were stressed with various bending radii (figures 1(*b*) and (*c*)). The bending direction was parallel to that of charge transport.

3. Results and discussion

Figure 2(*a*) shows the device characterization obtained under different mechanical bending conditions. Before the bending test, the device exhibited typical *p*-channel field effect behavior [14, 15]; the extracted mobility (μ) following the conventional field effect transistor model in the saturation regime was 0.17 cm^2 V^{-1} s^{-1}. The threshold voltage (V_t) and on–off ratio were −12.0 V and 10^4, respectively. Under either compressive or tensile strain with a bending radius of 10 mm, we only observed minor current change in the transfer curves (figure 2(*a*)). The threshold voltage slightly shifted positively by 0.30 V under compressive strain. On the other hand, the V_t shifted toward the negative direction by 0.45 V under tensile strain, suggesting that a higher driving voltage was required to turn on the channel conduction. From the output characteristics (figure 2(*b*)), we could more clearly tell that the drain current increased under compressive strain and decreased under the tensile condition. Further, the current differences increased with the gate voltage (V_G).

The strain on the substrate surface ($\varepsilon_{\text{surface}}$) at a certain bending curvature radius (R) can be expressed using the equation [16]

$$\varepsilon_{\text{surface}} = \left(\frac{d_f + d_s}{2R}\right) \frac{(1 + 2\eta + \chi\eta^2)}{(1+\eta)(1+\chi\eta)}, \qquad (1)$$

where d_f is the film thickness, d_s is the substrate thickness, $\eta = d_f/d_s$, $\chi = Y_f/Y_s$, and Y_f and Y_s are Young's moduli of the film and the substrate, respectively. Because d_f and d_s were ∼1.5 and 150 μm, respectively, we estimated η to be ∼0.01. Further, Young's modulus of organic materials usually ranges from 0.1 to 10 GPa [17], and the Y_s of SS substrates is ∼200 GPa [18]. Hence, χ should be quite small as well. Therefore, the strain ($\varepsilon_{\text{surface}}$) can be approximately determined as $d_s/2R$. Figure 3(*a*) displayed the normalized mobility with respect to the value obtained without bending as a function of the calculated strain. We can see that the mobility increased with increasing compressive strain and decreased with increasing tensile strain. More interestingly, we were able to fit a linear curve well to this set of data [19]. The slope of the fitting curve is 0.078 (%$^{-1}$), suggesting that 1% of compressive or tensile strain will lead to an increase

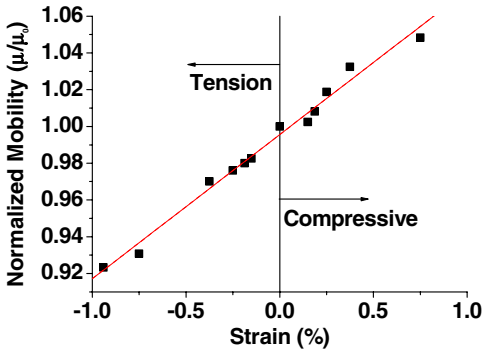

Figure 3. Mobility of the OTFTs as a function of strain. The initial values of mobility were normalized for ready comparison.

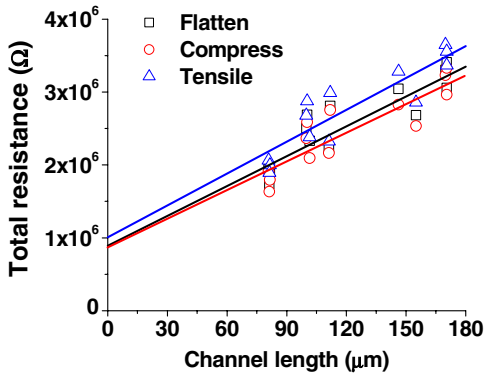

Figure 4. The device resistances as a function of channel length under different bending conditions. According to the transfer line method, the intercept of the fitting curve indicates the parasitic resistance.

or a decrease of ∼8% in mobility, respectively. Assuming the charge transport is thermal activated and governed by an Arrhenius-type equation, the mobility can be described as $\mu \sim \mu_0 \exp(-\Delta E/k_B T)$, where ΔE is the energy barrier for the charge hopping process [19, 20]. Therefore, we can estimate the effect of mechanical strain on ΔE in the flexible OTFTs as $\Delta E \propto -k_B T \ln(1+0.078\varepsilon)$, where strain ($\varepsilon$) is expressed in percent [19].

In order to further clarify the effect of mechanical bending, a transfer line method (TLM) [21] was adapted to analyze the resistance responses of the devices to the applied strain. In the linear regime, the total device turn-on resistance ($R_{\rm on}$) mainly comes from two contributions: the channel resistance ($R_{\rm ch}$) and the parasitic resistance (R_p) according to the following equation:

$$R_{\rm on} = \left(\frac{\partial V_{DS}}{\partial I_D}\right)_{V_{DS}\to 0}^{V_G=\text{const.}} = R_{\rm ch} + R_p$$
$$= \frac{L}{W\mu_i C_i (V_G - V_T)} + R_p. \qquad (2)$$

$R_{\rm on}$ could be calculated from the linear regime of the output curves (figure 2(*b*)). Because R_P is independent of the channel length, it can be extracted by plotting $R_{\rm on}$ as a function of channel length (L) (figure 4). The intercepts of the curves with the y-axis indicated the parasitic resistances. After knowing R_p, the channel resistance could be also deduced. From figure 4, the calculated R_P and $R_{\rm ch}$ before bending were 0.89 MΩ and 13.7 kΩ μm^{-1}, respectively. Under compressive strain, we can clearly see that the parasitic resistance only decreased slightly to 0.86 MΩ; the channel resistance decreased to 13.1 kΩ μm^{-1}. However, both R_P and $R_{\rm ch}$ under tensile strain increased to 1.01 MΩ and 14.6 kΩ μm^{-1}, respectively. In particular, we observed a large increase (∼12%) in the parasitic resistance under tensile strain.

To understand the origin of the increased R_P, we performed a so-called sticky tape test under either compressive or tensile strain with a bending radius of 10 mm [22]. As shown in figures 5(*a*) and (*b*), we found that the top Au source/drain electrodes of the devices could be much more easily removed under the tensile condition. Because Young's modulus of Au (∼80 GPa) is much larger than that of pentacene (∼15 GPa) [23], the strain of Au films was smaller than that of the pentacene layer under a similar shear stress. Therefore, as shown figure 5(*c*), we deduce that the source/drain electrodes tended to be delaminated, resulting in a poor contact. As a result, the contact resistance was increased under tensile strain. In contrast, the contact resistance reminded almost unchanged under the compressive bending condition, which was probably due to the opposite direction of the stress on the device layers.

Figure 6 shows the surface morphology of the pentacene layer, which exhibited typical polycrystalline morphology. For a polycrystalline TFT, the mobility is usually governed by the grain boundary mobility [24, 25]. In other words, the hopping process is usually limited by the activation energy barrier between the grains. Following the above assumption, we propose a model to explain the above observation which is as follows. Under a tensile strain (figure 6(*c*)), because the spacing between the gains probably becomes longer, the energy barrier between the grains is increased, thereby reducing the hopping rate of holes. On the other hand, when the substrates are under compressive strain, the grains come closer and, subsequently, the energy barrier is decreased (figure 6(*d*)). Therefore, we observed an increased mobility under an inward (compressive) bending condition.

Finally, we performed a cyclic bending test at a radius of 10 mm to examine the mechanical stability. During the bending test, the device was subject to either tensile or compressive strain. After bending, the electrical properties were measured in a flat state. Figure 7 reveals the normalized mobility as a function of bending times. For the device tested under compressive strain, the mobility gradually increased with bending cycles. On the other hand, the mobility of the device under tensile strain increased first and then decreased after ∼200 times of bending cycles. Further, after the applied bias was released, the mobility of the compressive device somehow recovered back to its origin value gradually, implying that the variation of the mobility was probably due to the polarization of the dielectric layer and/or adsorption of H_2O and O_2 from the atmosphere [26, 27]. On the other hand, for the tensile device, the damage of the source/drain contact might overwhelm the bias-stress effect in the beginning of the stress test, resulting in a decreased mobility. The two factors then probably became balanced and, therefore, the mobility

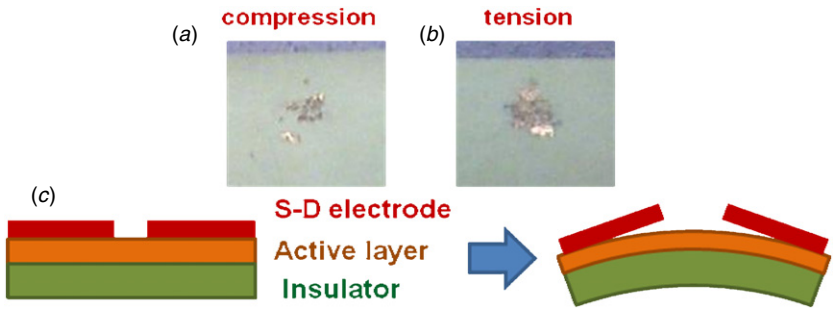

Figure 5. The pictures of the sticky tapes lifted-off from the device either under (*a*) compressive strain or (*b*) tensile strain. The bending radius was 10 mm. Note that more Au metal was removed under tensile strain. (*c*) The schematic representation of the cross-section of the device under the tensile strain condition.

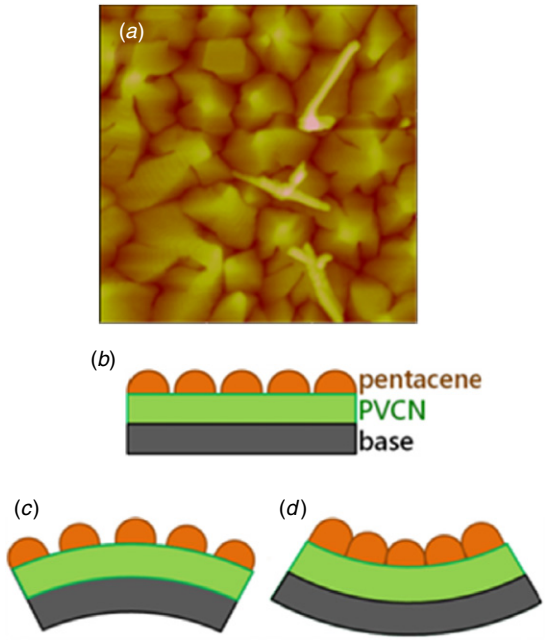

Figure 6. (*a*) The surface morphology of the pentacene layer. The schematic representation of the gains of the pentacene layer on a (*b*) flat substrate; (*c*) substrate under tensile strain; (*d*) substrate under compressive strain.

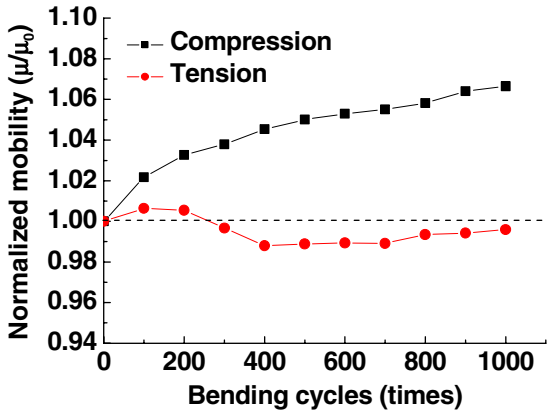

Figure 7. Variation of the normalized mobility as a function of bending cycles under either compressive or tensile strain.

became almost unchanged after ∼400 times of bending cycles.

4. Conclusion

We have investigated the effect of mechanical strain on pentacene thin-film transistors. The devices were fabricated on flexible stainless steel substrates and tested under different bending conditions. We observed that compressive strain resulted in an increased mobility, while tensile strain led to degraded electrical performance. We further used TLM to extract the channel and parasitic resistances under either compressive or tensile strain with a bending radius of 10 mm. The results indicated that the parasitic resistance increased by ∼12% under the tensile bending condition, which probably could be attributed to the damage of the source/drain contacts. Additionally, we deduced that mechanical strains influence the energy barrier height between the grains of pentacene thin films, thereby resulting in the variation of channel resistances. Finally, the fatigue test revealed that the OTFTs in this study exhibited supreme flexibility, especially under compressive bending conditions.

Acknowledgments

The authors thank the National Science Council (NSC 99-2221-E-009-181 and NSC 98-2218-E-009-002) and the Ministry of Education (though the ATU program) for financial support.

References

[1] Zaumseil J and Sirringhaus H 2007 *Chem. Rev.* **107** 1296
[2] Sung C F, Kekuda D, Chu L F, Lee Y Z, Chen F C, Wu M C and Chu C W 2009 *Adv. Mat.* **21** 4845
[3] Facchetti A, Yoon M H and Marks T J 2005 *Adv. Mat.* **17** 1705
[4] Subramanian V, Chang P C, Lee J B, Molesa S E and Volkman S K 2005 *IEEE Trans. Compon. Packag. Technol.* **28** 741
[5] Chung C S, Cheng J A, Huang Y J, Chang H F, Chen F C and Shieh H P D 2008 *Appl. Phys. Lett.* **93** 053305
[6] Kubozono Y, Haas S, Kalb W L, Joris P, Meng F, Fujiwara A and Batlogg B 2008 *Appl. Phys. Lett.* **93** 033316
[7] Tan H S, Kulkarni S R, Cahyadi T, Lee P S, Mhaisalkar S G, Kasim J, Shen Z X and Zhu F R 2008 *Appl. Phys. Lett.* **93** 183503
[8] Jedaa A and Halik M 2009 *Appl. Phys. Lett.* **95** 103309
[9] Wu C C, Theiss S D, Gu G, Lu M H, Sturm J C, Wagner S and Forrest S R 1997 *IEEE Electron Device Lett.* **18** 609
[10] Afentakis T, Hatalis M, Voutsas A T and Hartzell J 2006 *IEEE Trans. Electron Devices* **53** 815

[11] Chuang T K, Troccoli M, Kuo P C, Jamshidi-Roudbari A, Hatalis M K, Biaggio I and Voutsas A T 2007 *Appl. Phys. Lett.* **90** 151114
[12] Chen F C, Wu J L, Lee C L, Huang W C, Chen H M P and Chen W C 2009 *IEEE Electron Device Lett.* **30** 727
[13] Jang J, Kim S H, Hwang J, Nam S, Yang C, Chung D S and Park C E 2009 *Appl. Phys. Lett.* **95** 073302
[14] Chen F C, Chung C S, Lin Y S, Kung L J, Chen T H and Shieh H P D 2006 *Org. Electron.* **7** 435
[15] Chen F C, Chen Y P, Huang Y J and Chien S C 2010 *J. Phys. D: Appl Phys.* **43** 405103
[16] Won S H, Chung J K, Lee C B, Nam H C, Hur J H and Jin J 2004 *J. Electrochem. Soc.* **151** G167
[17] Stuart B H 2002 *Polymer Analysis* (England: Wiley)
[18] Peng I H, Liu P T and Wu T B 2009 *Appl. Phys. Lett.* **95** 041909
[19] Sekitani T, Kato Y, Iba S, Shinaoka H, Someya T, Sakurai T and Takagi S 2005 *Appl. Phys. Lett.* **86** 073511
[20] Horowitz G 2003 *Adv. Funct. Mater.* **13** 53
[21] Necliudov P V, Shur M S, Gundlach D J and Jackson T N 2003 *Solid-State Electron.* **47** 259
[22] Ma W, Yang C, Gong X, Lee K and Heeger A J 2005 *Adv. Funct. Mater.* **15** 1617
[23] Tahk D, Lee H H and Khang D Y 2009 *Macromolecules* **42** 7079
[24] Horowitz G, Hajlaoui M E and Hajlaoui R 2000 *J. Appl. Phys.* **87** 4456
[25] Annibale P, Albonetti C, Stoliar P and Biscarini F 2007 *J. Phys. Chem.* A **111** 12854
[26] Jung T, Dodabalapur A, Wenz R and Mohapatra S 2005 *Appl. Phys. Lett.* **87** 182109
[27] Chen F C and Liao C H 2008 *Appl. Phys. Lett.* **93** 103310